Study of Secondary Field Waves at Scattering of Nonlinearly Interacting Acoustic Waves by an Elongated Spheroid

Iftikhar B. Abbasov

Taganrog Technological Institute of the Southern Federal University, Nekrasovskyi 44, Taganrog, 347928, Russia

(Received 25 October 2013; revised 1 April 2008; accepted 6 October 2014)

The study and three-dimensional simulation of the field of the second harmonic wave at the scattering of nonlinearly interacting acoustic waves by an elongated spheroid are carried out in this work. The problem is presented in the elongated spheroidal coordinate system, and the foci of the spheroid coincide with foci of the spheroidal coordinate system. The description of the occurring wave processes is presented on the basis of the obtained relation for acoustic pressure of the second harmonic wave. The scattering diagrams for the acoustic pressure field of the second harmonic wave are presented, and three-dimensional models of a scattering diagram are created.

1. INTRODUCTION

The problem of acoustic waves scattering by elongated spheroids was formulated for the first time about half a century ago.[1–3] Some of this research considered the problem of the sound scattering by an elongated spheroid with different boundary conditions.[1] Other research considered the problem of the sound scattering by a rigid spheroid in the long-wave approximation.[2] And other work is devoted to the problem of sound waves scattering by an elongated spheroid.[3] The angular characteristics of the acoustic waves scattering by a soft and rigid elongated spheroid were presented.

The process of the plane acoustic waves scattering by thin, acoustically rigid and resilient bodies of revolution was considered in some of the research used in this study.[4,5] In other works, the problem of the plane acoustic wave scattering by spheroidal shells was investigated.[6,7] These works study the surface waves directly on scatterers, and the frequency dependence of the backscattering amplitude in the far field is presented. With the exception of the works on the linear scattering by spheroids, there are several papers devoted to nonlinear acoustic spectroscopy. Some studies used here consider the problem of nonlinear acoustic diagnostics of defects in materials and structures.[8] Other research presented here is devoted to solving the problem of the nonlinear acoustic spectroscopy of defects in geomaterials.[9]

However, the problem of interacting nonlinear acoustic waves scattered by an elongated spheroid has not been examined elsewhere. This problem becomes essential when an acoustic parametric antenna is used for remote diagnostics of a water medium, as well as in the medical tomography field.

In the present work, the study and simulation of the secondary field of the second harmonic wave is carried out. The study of the secondary field of the difference-frequency wave for nonlinearly interacting plane acoustic waves scattered by a rigid elongated spheroid was also performed.[10] However, the scattering process for the high-frequency second harmonic wave has a purely geometrical character ($k_{2\omega}h_0 \gg 1$). But the difference-frequency wave covers the Rayleigh- ($k_{-}h_0 \ll 1$) and resonance- ($k_{-}h_0 \approx 1$) scattering regions. A multi-frequency analysis will lead to an increase in informativeness of the scattered signal.

2. STATEMENT OF PROBLEM

The problem of wave diffraction by elongated bodies is often described in ellipsoidal coordinates. These coordinates are used in the study of radiation and the scattering of acoustic waves by ellipsoids, or cigar-shaped bodies, and when studying the diffraction by circular apertures.[11]

The elongated spheroidal coordinate system, ξ, η, and φ, is used for the study of diffraction by cigar-shaped bodies . The foci of the spheroid coincide with foci of the spheroidal coordinate system. The spheroid is formed by rotating the ellipse ξ_0 around its major axis, which coincides with the x-axis in the Cartesian coordinate system. The geometry of the problem is presented in Fig. 1. The $\xi = const$ spheroids and $\eta = const$ two-sheeted hyperboloids are the coordinate surfaces in this case.

Elongated spheroidal coordinates are related to Cartesian coordinates by the following equations:[12]

$$x = h_0\xi\eta, \qquad y = h_0\sqrt{(\xi^2-1)(1-\eta^2)}\cos\varphi,$$
$$z = h_0\sqrt{(\xi^2-1)(1-\eta^2)}\sin\varphi;$$

where $h_0 = d/2$ and d is the interfocal distance. Spheroidal coordinates ξ, η, and φ vary within the limits $1 \le \xi < \infty$; $-1 \le \eta \le 1$; and $0 \le \varphi \le 2\pi$.

The perfect elongated spheroid is placed into a homogeneous medium. The spheroid's surface is characterized by the radial coordinate ξ_0. In our case, the spheroid is supposed to be acoustically rigid. Consequently, the Neumann boundary

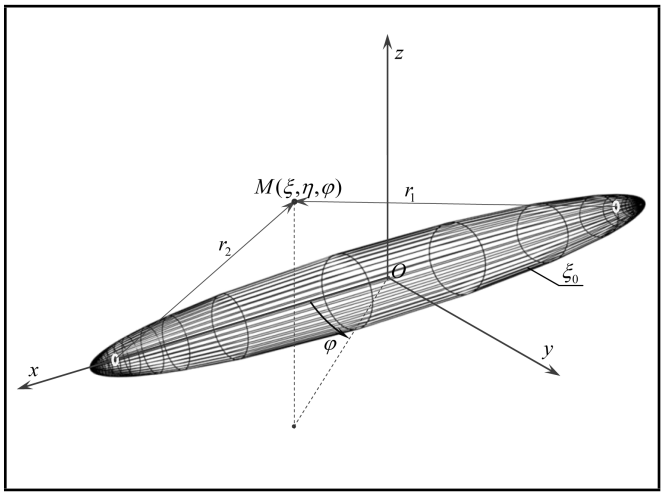

Figure 1. Geometry of the problem.

condition is satisfied at the surface. We assume that interacting high-frequency plane acoustic waves of the unit pressure amplitude fall onto the spheroid at an arbitrary polar angle θ_0 ($\theta_0 = \arccos\eta_0$) and an azimuthal angle φ_0 in the spheroidal coordinate system:[11]

$$p_{ni} = \exp\left[-i(k_n r_0\cos\theta_0 - \omega_n t)\right] = -2\exp(i\omega_n t)\sum_{m=0}^{\infty}\sum_{l\geq m}^{\infty} i^{-l}\overline{S_{ml}}(k_n h_0,\eta_0)\overline{S_{ml}}(k_n h_0,\eta)\cdot R_{ml}^{(1)}(k_n h_0,\xi)\cos m(\varphi-\varphi_0); \quad (1)$$

where k_n is the wavenumber; $n = 1, 2$ according to the waves with frequencies ω_1 and ω_2; r_0 is the radius-vector of the polar coordinate system; $\overline{S_{ml}}(k_n h_0,\eta)$ is the normalized angular first-order function; and $R_{ml}^{(1)}(k_n h_0,\xi)$ is the radial spheroidal first-order function.

After the plane wave scattering by the spheroid, the scattered spheroidal wave with pressure[3] will propagate in the environment

$$p_{ns}(\xi,\eta,\varphi) = 2\exp(i\omega_n t)\sum_{m=0}^{\infty}\sum_{l\geq m}^{\infty} A_{ml}(k_n h_0,\xi_0)\cdot \overline{S_{ml}}(k_n h_0,\eta)R_{ml}^{(3)}(k_n h_0,\xi)\cos m\varphi; \quad (2)$$

where $A_{ml}(k_n h_0,\xi_0)$ is the coefficient dependent on boundary conditions on the spheroid surface, and $R_{ml}^{(3)}(k_n h_0,\xi)$ is the radial spheroidal third-order function.

When the scattered spheroidal wave occurs, the total acoustic pressure of the primary field around the spheroid will be

$$p^{(1)} = p_{ni} + p_{ns} = \left[\sum_{m=0}^{\infty}\sum_{l\geq m}^{\infty} B_{ml}(k_n h_0)\exp\left[i(\omega_n t - l\pi/2)\right] + \sum_{m=0}^{\infty}\sum_{l\geq m}^{\infty} D_{ml}(k_n h_0)\exp\left[i(\omega_n t - m\varphi)\right]\right] + (c.c.); \quad (3)$$

where

$$B_{ml}(k_n h_0) = 2\overline{S_{ml}}(k_n h_0,\eta_0)\overline{S_{ml}}(k_n h_0,\eta)R_{ml}^{(1)}(k_n h_0,\xi)\cdot\cos m(\varphi-\varphi_0),$$

$$D_{ml}(k_n h_0) = 2A_{ml}(k_n h_0,\xi_0)\overline{S_{ml}}(k_n h_0,\eta)R_{ml}^{(3)}(k_n h_0,\xi)\cdot\cos m\varphi,$$

and $(c.c.)$ is the complex-conjugate part.

When solving problems of nonlinear interaction, it is necessary to take into account the reality of sound pressure; therefore, Eq. (3) is presented with the complex-conjugated part.

The nonlinear wave processes around the spheroid can be described by the inhomogeneous wave equation[13]

$$\Delta p^{(2)} - \frac{1}{c_0^2}\frac{\partial^2 p^{(2)}}{\partial t^2} = -Q = -\frac{\varepsilon}{c_0^4\rho_0}\frac{\partial^2 p^{(1)}}{\partial t^2}; \quad (4)$$

where Q is the volume density of the sources of secondary waves, c_0 is the sound velocity in the medium, ε is the quadratic nonlinearity parameter, ρ_0 is the density of the unperturbed medium, and $p^{(1)}$ and $p^{(2)}$ are the total acoustic pressures of the primary and secondary fields.

The wave in Eq. (4) is solved by the method of successive approximations. In the first approximation, the solution is represented by Eq. (3) for the total acoustic pressure of the primary field $p^{(1)}$. To find the solution in the second approximation, $p^{(2)}$, the right side of Eq. (4) should feature four frequency components: second harmonics of the incident waves, $2\omega_1$, $2\omega_2$, and the combination frequency waves, $\omega_1 + \omega_2$, $\omega_2 - \omega_1 = \Omega$.

The equation for the volume density of secondary waves sources $Q_{2\omega}$ at the second harmonic $2\omega_1$ is

$$Q_{2\omega} = \frac{8\varepsilon\omega_1^2}{c_0^4\rho_0}\left[\sum_{m=0}^{\infty}\sum_{l\geq m}^{\infty} B_{ml}^2(k_1 h_0)\cos(2\omega_1 t - l\pi) + \sum_{m=0}^{\infty}\sum_{l\geq m}^{\infty} 2B_{ml}(k_1 h_0)D_{ml}(k_1 h_0)\cos(2\omega_1 t - l\pi/2 - m\varphi) + \sum_{m=0}^{\infty}\sum_{l\geq m}^{\infty} D_{ml}^2(k_1 h_0)\cos(2\omega_1 t - 2m\varphi)\right]. \quad (5)$$

3. SOLUTION OF NONLINEAR WAVE EQUATION FOR THE SECOND HARMONIC WAVE

To solve the inhomogeneous wave shown in Eq. (4) with the right-hand side given by Eq. (6) in the second approximation, we seek the solution in the complex form

$$p_{2\omega}^{(2)} = \frac{1}{2}P_{2\omega}^{(2)}\exp\big(i(2\omega_1 t + \delta)\big) + (c.c.). \quad (6)$$

The inhomogeneous Helmholtz equation is obtained by supplanting Eq. (6) into the inhomogeneous wave Eq. (4):

$$\Delta P_{2\omega}^{(2)} + k_{2\omega}^2 P_{2\omega}^{(2)} = -q_{2\omega}(\xi,\eta,\varphi); \quad (7)$$

where $k_{2\omega}^2 = 2k_1$ is the wavenumber of the second harmonic $2\omega_1$, and $q_{2\omega}(\xi,\eta,\varphi)$ is the function of the sources of secondary waves

$$q_{2\omega}(\xi,\eta,\varphi) = \frac{8\varepsilon\omega_1^2}{c_0^4\rho_0}\Bigg[\sum_{m=0}^{\infty}\sum_{l\geq m}^{\infty} B_{ml}^2(k_1h_0)\exp\big(i(2\omega_1 t - l\pi)\big) + \sum_{m=0}^{\infty}\sum_{l\geq m}^{\infty} 2B_{ml}(k_1h_0)D_{ml}(k_1h_0)\exp\big(i(2\omega_1 t - l\pi/2 - m\varphi)\big) + \sum_{m=0}^{\infty}\sum_{l\geq m}^{\infty} D_{ml}^2(k_1h_0)\exp\big(i(2\omega_1 t - 2m\varphi)\big)\Bigg].$$

The solution to the inhomogeneous Helmholtz equation in Eq. (7) takes the form of a volume integral of the product of the Green's function with the secondary wave sources density[13, 14]

$$P_{2\omega}^{(2)}(\xi,\eta,\varphi) = \int_V q_{2\omega}(\xi',\eta',\varphi')G(r_1)h_{\xi'}h_{\eta'}h_{\varphi'}\,d\xi'd\eta'd\varphi'; \tag{8}$$

where $G(r_1)$ is the Green function, r_1 is the distance between the current point of the volume $M'(\xi',\eta',\varphi')$ and the observation point $M(\xi,\eta,\varphi)$, and $h_{\xi'}$, $h_{\eta'}$, $h_{\varphi'}$ are the scale factors (coefficients of Lame).[15]

The Green's function in the far zone $r' \ll r$ is determined by the asymptotic equation

$$G(r_1) \approx \exp\Big[-ik_{2\omega}\Big(h_0\xi - h_0\xi'\eta\eta' - h_0\xi'\sqrt{(1-\eta^2)(1-\eta'^2)}\times\cos(\varphi-\varphi')\Big)\Big]\Big/h_0\xi. \tag{9}$$

The integration in Eq. (8) is performed over the volume V occupied by the second wave sources and bounded in the spheroidal coordinates by relations $\xi_0 \leq \xi' \leq \xi_S$, $-1 \leq \eta' \leq 1$, $0 \leq \varphi' \leq 2\pi$.

This volume represents a spheroidal layer of the medium, stretching from the spheroidal scatterer surface to the boundary of the nonlinear interaction area. A spheroidal surface with the coordinate ξ_S is the boundary of this area. The coordinate ξ_S is defined by the length of the nonlinear interaction area (attenuation area) of the initial high-frequency waves. The length of this area is inversely proportional to the coefficient of viscous sound absorption at the corresponding pumping frequency. The scattered waves' interaction can be neglected due to attenuation beyond this area. For the interacting incident waves, the boundary introduction is equivalent to placing the absorption filter at the boundary.

As a result of the final integration over coordinates φ' and η' when taking into account the equation for the sources of secondary waves, Eq. (8) takes the form[16]

$$P_{2\omega}^{(2)}(\xi,\eta,\varphi) = P_{2\omega\mathrm{I}}^{(2)}(\xi,\eta,\varphi) + P_{2\omega\mathrm{II}}^{(2)}(\xi,\eta,\varphi) + P_{2\omega\mathrm{III}}^{(2)}(\xi,\eta,\varphi) = C_{2\omega}\frac{1}{k_{2\omega}h_0\eta}\Bigg[\int_{\xi_0}^{\xi_S} T\xi'\sin(k_{2\omega}h_0\xi'\eta)d\xi' - \int_{\xi_0}^{\xi_S} T\frac{\sin(k_{2\omega}h_0\xi'\eta)}{\xi'}d\xi'\Bigg]; \tag{10}$$

where

$$C_{2\omega} = \frac{32\pi h_0^3\varepsilon\omega_1^2\exp(-ik_{2\omega}h_0\xi)}{c_0^4\rho_0\xi},$$

$$T = \Bigg[\sum_{m=0}^{\infty}\sum_{l\geq m}^{\infty} B_{ml}^2(k_1h_0)\exp(-il\pi) + \sum_{m=0}^{\infty}\sum_{l\geq m}^{\infty} 2B_{ml}(k_1h_0)D_{ml}(k_1h_0)\exp\big(-i(l\pi/2+m\varphi)\big) + \sum_{m=0}^{\infty}\sum_{l\geq m}^{\infty} D_{ml}^2(k_1h_0)\exp(-2im\varphi)\Bigg],$$

(and from here on, the time factor $\exp(i2\omega_1 t)$ is omitted).

In contrast with the different frequency wave in Eq. (10), the total acoustic pressure of the second harmonic wave $P_{2\omega}^{(2)}(\xi,\eta,\varphi)$ consists of three spatial components. Therefore, the contribution of the separate components in the total field will increase.

The first component, $P_{2\omega\mathrm{I}}^{(2)}(\xi,\eta,\varphi)$, corresponds with the part of the total acoustic pressure of the second harmonic wave, which is formed in the spheroidal layer of the nonlinear interaction area by the incident high-frequency plane wave ω_1. The second component, $P_{2\omega\mathrm{II}}^{(2)}(\xi,\eta,\varphi)$, describes the interaction of the incident plane wave with the scattered spheroidal wave of frequency ω_1. The third component, $P_{2\omega\mathrm{III}}^{(2)}(\xi,\eta,\varphi)$, characterizes the self-interaction of the scattered spheroidal wave of frequency ω_1. It should also be noted that these components characterize the nonlinear interaction of incident and scattered waves with different spatial configurations of the wave fronts.

After the final integration over the coordinate ξ', the equation for the first component $P_{2\omega\mathrm{I}}^{(2)}(\xi,\eta,\varphi)$ takes the following form:

$$P_{2\omega\mathrm{I}}^{(2)}(\xi,\eta,\varphi) = P_{2\omega\mathrm{I}1}^{(2)} + P_{2\omega\mathrm{I}2}^{(2)} + P_{2\omega\mathrm{I}3}^{(2)} + P_{2\omega\mathrm{I}4}^{(2)}; \tag{11}$$

where

$$P_{2\omega\mathrm{I}1,2\omega\mathrm{I}2}^{(2)} = \pm\frac{C_{2\omega}}{2k_{2\omega}^2h_0^2\eta(\eta_0\mp\eta)}\cdot \Big[\xi_S\exp\big[-ik_{2\omega}h_0(\eta_0\mp\eta)\xi_S\big] - \xi_0\exp\big[-ik_{2\omega}h_0(\eta_0\mp\eta)\xi_0\big]\Big],$$

$$P_{2\omega\mathrm{I}3,2\omega\mathrm{I}4}^{(2)} = \mp\frac{C_{2\omega}}{2i(k_{2\omega}h_0\eta)}\cdot \Big[-\mathrm{Ei}\big[-ik_{2\omega}h_0(\eta_0\mp\eta)\xi_S\big] + \mathrm{Ei}\big[-ik_{2\omega}h_0(\eta_0\mp\eta)\xi_0\big]\Big],$$

and $\mathrm{Ei}(ax) = \int \frac{\exp(ax)}{x}$ is the integral exponential function.[17,18]

Analysing what was obtained in Eq. (11) for the first component, $P^{(2)}_{2\omega\mathrm{I}}(\xi,\eta,\varphi)$, of the total acoustic pressure of the second harmonic wave, one can note that the scattering diagram of this component is determined by the behaviour of the function $1/(\eta_0 \pm \eta)$. This function depends on the coordinate η_0, i.e. on the angle of incidence θ_0 of the high-frequency plane waves in the polar coordinate system.

Now consider the second component of Eq. (10), $P^{(2)}_{2\omega\mathrm{II}}(\xi,\eta,\varphi)$, for the total acoustic pressure of the second harmonic wave, which characterizes the nonlinear interaction of the incident plane wave with the scattered spheroidal wave. After the final integration, the equation for the second component of the total acoustic pressure of the second harmonic wave takes the form

$$P^{(2)}_{2\omega\mathrm{II}}(\xi,\eta,\varphi) = P^{(2)}_{2\omega\mathrm{II}1} + P^{(2)}_{2\omega\mathrm{II}2} + P^{(2)}_{2\omega\mathrm{II}3} + P^{(2)}_{2\omega\mathrm{II}4}; \quad (12)$$

where

$$P^{(2)}_{2\omega\mathrm{II}1,2\omega\mathrm{II}2} = \mp \frac{iC_{2\omega}A(k_1k_0)}{2k_1k_{2\omega}h_0^2\eta\sqrt{(1-\eta_0)(1-\eta)}} \cdot \left[\frac{\exp(-iu_{2\omega}\xi_S) - \exp(-iu_{2\omega}\xi_0)}{u_{2\omega}}\right],$$

$$P^{(2)}_{2\omega\mathrm{II}3,2\omega\mathrm{II}4} = \pm \frac{C_{2\omega}A(k_1k_0)}{2k_1k_{2\omega}h_0^2\eta\sqrt{(1-\eta_0)(1-\eta)}} \cdot \left[\frac{\exp(-iu_{2\omega}\xi_S)}{\xi_S} - \frac{\exp(iu_{2\omega}\xi_0)}{\xi_0} - iu_{2\omega}\left[\mathrm{Ei}(-iu_{2\omega}\xi_S) - \mathrm{Ei}(-iu_{2\omega}\xi_0)\right]\right],$$

and $u_{2\omega} = (k_1h_0\eta - k_1h_0 \mp k_{2\omega}h_0\eta)$.

An analysis of Eq. (12) shows that the scattering diagrams of the second component $P^{(2)}_{2\omega\mathrm{II}}(\xi,\eta,\varphi)$ are determined mainly by the function $1/\eta\sqrt{(1-\eta_0)(1-\eta)}$, where the dependence on the incident angle θ_0 (that is η_0) is not very pronounced.

Now, we consider the third component of Eq. (10), $P^{(2)}_{2\omega\mathrm{III}}(\xi,\eta,\varphi)$, for the total acoustic pressure of the second harmonic wave, characterizing the nonlinear self-interaction of the scattered spheroidal wave frequency ω_1. After the final integration, the equation for the third component of the total acoustic pressure of the second harmonic wave takes the form

$$P^{(2)}_{2\omega\mathrm{III}}(\xi,\eta,\varphi) = P^{(2)}_{2\omega\mathrm{III}1} + P^{(2)}_{2\omega\mathrm{III}2} + P^{(2)}_{2\omega\mathrm{III}3} + P^{(2)}_{2\omega\mathrm{III}4}; \quad (13)$$

where

$$P^{(2)}_{2\omega\mathrm{III}1,2\omega\mathrm{III}2} = \mp \frac{C_{2\omega}A^2(k_1k_0)}{2ik_{2\omega}h_0^3k_1^2\eta(1-\eta_0)(1-\eta)} \cdot \left[-u_{3\omega}\left[\mathrm{Ei}(-iu_{3\omega}\xi_S) - \mathrm{Ei}(-iu_{3\omega}\xi_0)\right]\right],$$

$$P^{(2)}_{2\omega\mathrm{III}3,2\omega\mathrm{III}4} = \mp \frac{C_{2\omega}A^2(k_1k_0)}{4ik_{2\omega}h_0^3k_1^2\eta(1-\eta_0)(1-\eta)} \cdot \left[iu_{3\omega}\left(\frac{\exp(-iu_{3\omega}\xi_S)}{\xi_S} - \frac{\exp(iu_{3\omega}\xi_0)}{\xi_0}\right) + u_{3\omega}^2\left[\mathrm{Ei}(-iu_{3\omega}\xi_S) - \mathrm{Ei}(-iu_{3\omega}\xi_0)\right]\right],$$

and $u_{3\omega} = (k_{2\omega}h_0 \mp k_{2\omega}h_0\eta)$.

The scattering diagrams type is defined mainly by the function $1/\eta(1-\eta_0)(1-\eta)$ of Eq. (13).

4. DRAWING OF SCATTERING DIAGRAMS

To reveal the features of the acoustic field of the second harmonic wave, we consider the scattering diagrams for separate spatial components. The diagrams of the second harmonic wave components $P^{(2)}_{2\omega}(\xi,\eta,\varphi)$ scattered by a rigid elongated spheroid $\xi_0 = 1.005$ are presented in Fig. 2 (relation axis 1:10, $h_0 = 0.01$ m, distance from focal points $r_1 = 0.01$ m, $r_2 = 0.0101$ m) at: $\xi = 7$, angle of incidence shown an arrow $\theta_0 = 30^\mathrm{o}$, $f_2 = 1000$ kHz, $f_1 = 976$ kHz ($k_{1,2}h_0 \approx 40$), $2f_1 = 1952$ kHz, $k_{2\omega}h_0 = 82$, ($k_-h_0 = 1$). The initial parameter values of the second harmonic wave are connected to values for the difference-frequency wave.[10]

The scattering diagram for the first component $P^{(2)}_{2\omega\mathrm{I}}(\xi,\eta,\varphi)$ has maxima in the direction of the angle of incidence and in the symmetrical (with respect to the z-axis) direction (30^o and 150^o). The diagrams of other components have major maxima in the reverse and lateral directions (0^o and $\pm 90^\mathrm{o}$) and do not show dependence on the angle of incidence.

The scattering diagrams for the second harmonic wave $P^{(2)}_{2\omega}(\xi,\eta,\varphi)$ on a rigid elongated spheroid $\xi_0 = 1.005$ ($h_0 = 0.01$ m) for different radial distance values ξ are presented in Fig. 3 (the size of the re-radiating volume) at: $\theta_0 = 30^\mathrm{o}$, $f_2 = 1000$ kHz, $f_1 = 976$ kHz, ($k_{1,2}h_0 \approx 40$), $2f_1 = 1952$ kHz, $k_{2\omega}h_0 = 82$ ($k_-h_0 = 1$), $\xi = 3; 7; 15$.

The scattering diagrams for different wave dimensions of the spheroid and for different sizes of the interaction area were calculated. As a result, it was found that increasing the wave dimension of the spheroidal scatterer leads to minor changes in the maxima levels (in contrast with the difference-frequency wave). An increase in the size of the interaction area around the elongated spheroidal scatterer (coordinates ξ) leads to narrowing of these maxima.

In Fig. 4 are presented the scattering diagrams of the second harmonic wave $P^{(2)}_{2\omega}(\xi,\eta,\varphi)$ by a rigid elongated spheroid $\xi_0 = 1.005$ ($h_0 = 0.01$ m) for the different incidence angle values of the initial pumping waves $\theta_0 = 0^\mathrm{o}; 60^\mathrm{o}; 90^\mathrm{o}$ ($f_2 = 1000$ kHz, $f_1 = 976$ kHz, ($k_{1,2}h_0 \approx 40$), $2f_1 = 1952$ kHz, $k_{2\omega}h_0 = 82$ ($k_-h_0 = 1$), $\xi = 7$).

The scattering diagrams of the second harmonic wave $P^{(2)}_{2\omega}(\xi,\eta,\varphi)$ for the different incidence angle values $\theta_0 = 0^\mathrm{o}; 60^\mathrm{o}; 90^\mathrm{o}$ reproduce the features of the scattering diagrams of the difference-frequency wave $P^{(2)}_{-}(\xi,\eta,\varphi)$.

The scattering diagram of the second harmonic wave retains the general regularity in directions to the maxima. However, unlike the difference-frequency wave, the diagram does not undergo significant changes for different values of the spheroid's wave dimensions in accordance with the maxima, and it has more sharpened maxima. These features are associated with the geometric character of the scattering process.

Figures 5 and 6 show spatial models of the scattering diagrams of the second harmonic wave $P^{(2)}_{2\omega}(\xi,\eta,\varphi)$ by a rigid

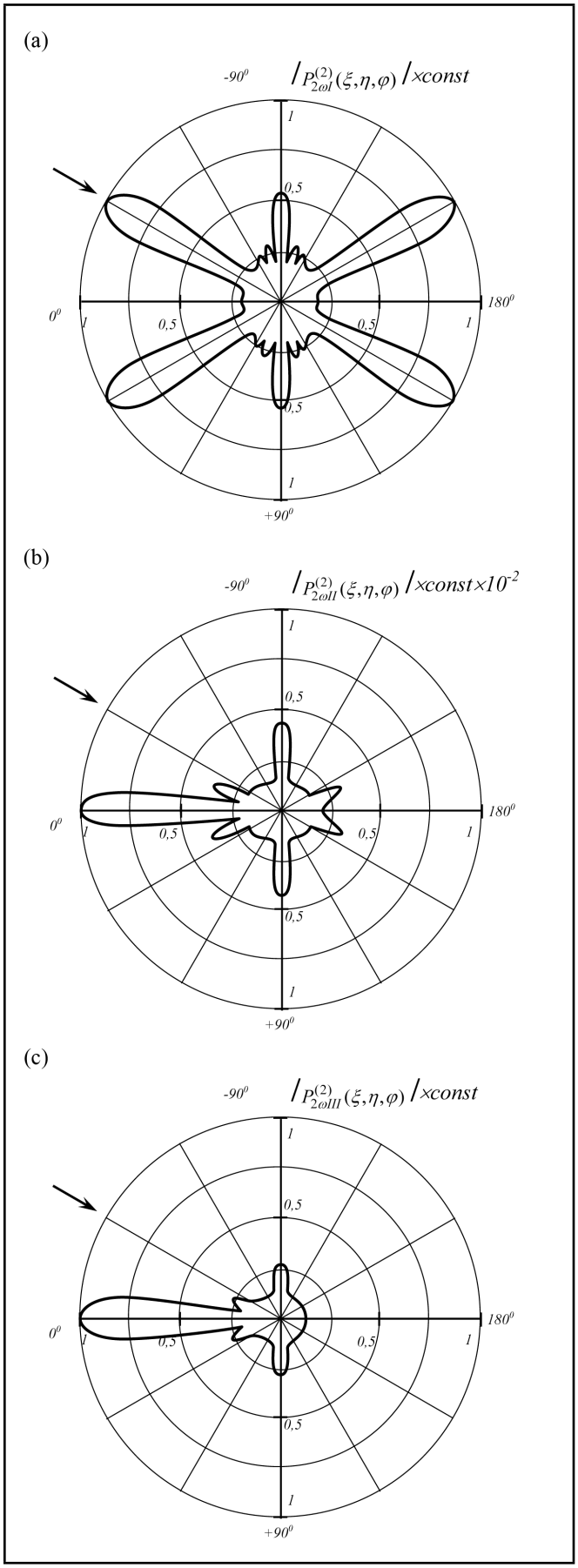

Figure 2. Scattering diagrams for the second harmonic wave $P^{(2)}_{2\omega}(\xi,\eta,\varphi)$ components on a rigid elongated spheroid $\xi_0 = 1.005$ for: $\xi = 7$, $\theta_0 = 30^{\rm o}$, $f_2 = 1000$ kHz, $f_1 = 976$ kHz, $2f_1 = 1952$ kHz, $k_{2\omega}h_0 = 82$ ($k_- h_0 = 1$).

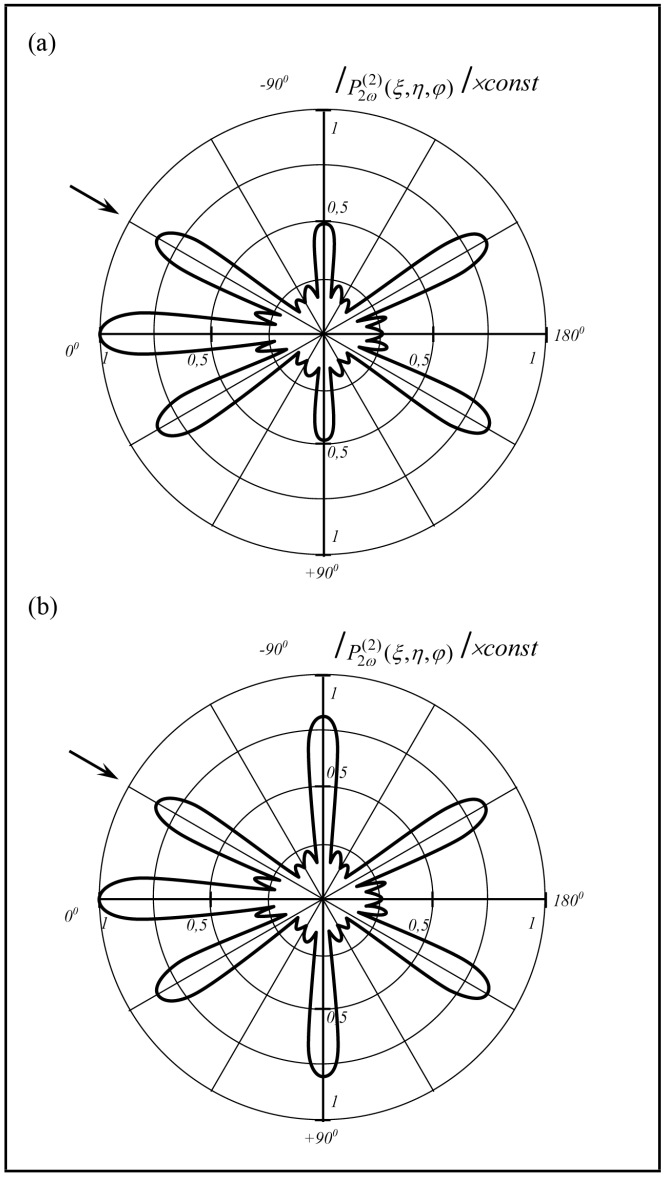

Figure 3. Scattering diagrams of the second harmonic wave $P^{(2)}_{2\omega}(\xi,\eta,\varphi)$ on a rigid elongated spheroid $\xi_0 = 1.005$ for different ξ values for: $f_2 = 1000$ kHz, $f_1 = 976$ kHz, $2f_1 = 1952$ kHz, $k_{2\omega}h_0 = 82$, $\theta_0 = 30^{\rm o}$, $\xi = 3; 7; 15$.

elongated spheroid $\xi_0 = 1.005$ for the angle of incidence $\theta_0 = 0^{\rm o}; 30^{\rm o}$. These diagrams provide a visual representation of the spatial distribution of the scattered pressure field.

5. DISCUSSION AND COMPARISON OF RESULTS

Further, it should be noted that the acoustic pressure of the second harmonic wave was calculated in the far field of the spheroidal scatterer, in the Fraunhofer zone. Therefore, the scattering field can be considered to be formed since the observation point $M(\xi,\eta,\varphi)$ was located at the radial distance $\xi = 7$ and 15. This distance exceeds 3 to 5 times the quasi-diffraction zone length.

The scattering diagrams are shown in the plane xOz. The polar angle θ varies in the range from $0^{\rm o}$ to $\pm 180^{\rm o}$ since the diagrams are axisymmetric with respect to the x-axis. The value

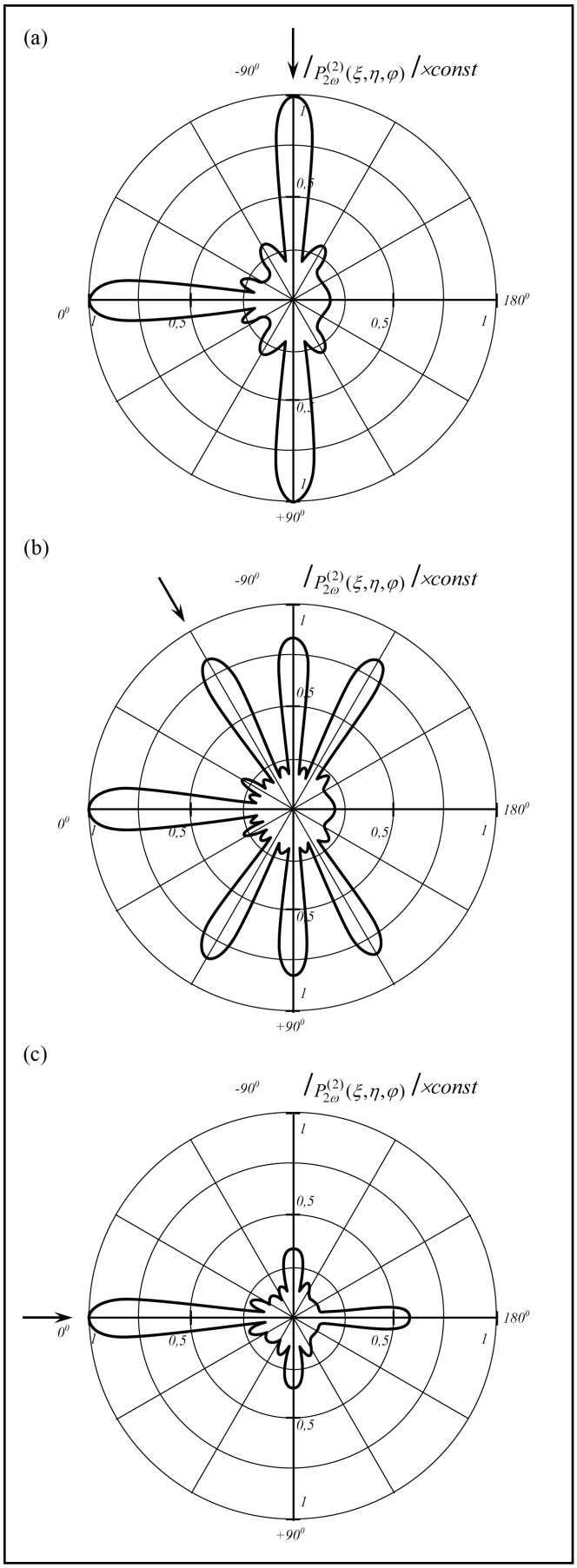

Figure 4. Scattering diagrams of the second harmonic wave $P_{2\omega}^{(2)}(\xi,\eta,\varphi)$ on a rigid elongated spheroid $\xi_0 = 1.005$ for angles of incidence $\theta_0 = 0^{\rm o}; 60^{\rm o}; 90^{\rm o}$ for: $f_2 = 1000$ kHz, $f_1 = 976$ kHz, $2f_1 = 1952$ kHz, $k_{2\omega}h_0 = 82$ ($k_- h_0 = 1$), $\xi = 7$.

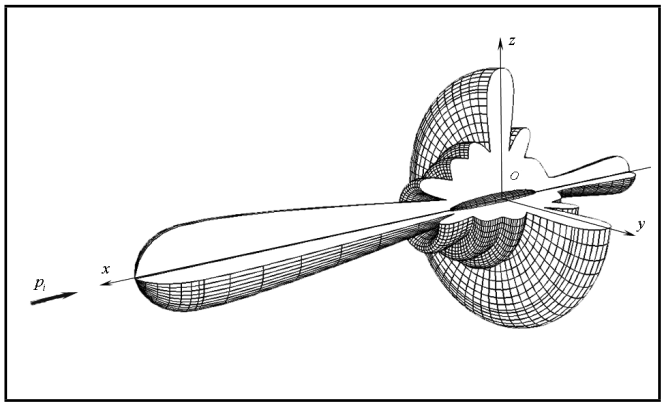

Figure 5. Three-dimensional wireframe model of scattering diagram of the second harmonic wave $P_{2\omega}^{(2)}(\xi,\eta,\varphi)$ on a rigid elongated spheroid $\xi_0 = 1.005$ at the angle of incidence $\theta_0 = 0^{\rm o}$ ($k_{2\omega}h_0 = 82$, $\xi = 7$).

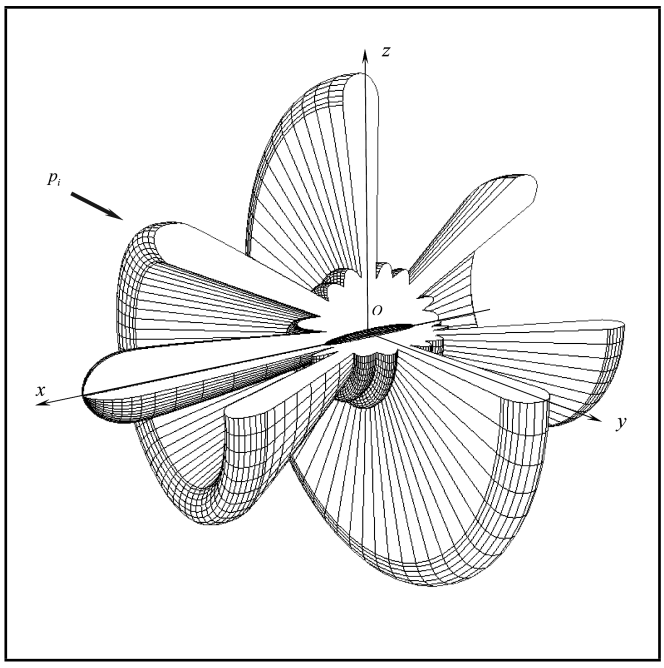

Figure 6. Three-dimensional wireframe model of scattering diagram of the second harmonic wave $P_{2\omega}^{(2)}(\xi,\eta,\varphi)$ on a rigid elongated spheroid $\xi_0 = 1.005$ at the angle of incidence $\theta_0 = 30^{\rm o}$ ($k_{2\omega}h_0 = 74$, $\xi = 3$).

of the angle $\theta = 0^{\rm o}$ corresponds to the axis x position, and the value $\theta = 90^{\rm o}$ corresponds to the z-axis. The arrow shows the direction of the initial plane waves' incidence.

For clarity, the figures show the acoustic pressure $P_{2\omega}^{(2)}(\xi,\eta,\varphi)$ dependence not on the angle of the hyperbola's asymptote η, but on more convenient polar angle $\theta = \arccos\eta$ in spherical coordinates. This representation is conventionally employed for the scattering diagrams in spheroidal coordinates.[2,3,19]

In order to check the correctness of the obtained diagrams of scattering by an elongated spheroid, we should compare them with the results of other studies. It should be also noted that the problem in the nonlinear formulation was not previously investigated, neither theoretically nor experimentally. Within the framework of our consideration, in the case of primary high-frequency waves, the scattering by a spheroid is linear. The secondary field is generated by the secondary wave sources lo-

cated in the volume around the spheroid. In the linear case, they are located on the spheroid's surface. In general, it can be emphasized that the obtained scattering diagrams are in good agreement with diagrams in the works cited in this paper.[3,5,20]

In the far field, the spheroidal coordinates are transformed into the spherical ones $P_+^{(2)}(\xi,\eta,\varphi) \to P_+^{(2)}(r,\theta,\varphi)$. The diagrams of scattering by an elongated spheroid in the far field are in good agreement with the author's study results on scattering by a sphere.[21,22] However, unlike the case of a sphere, where the scattered field does not depend on the angle of incidence θ, the lobes in the directions of incidence and reflection of the initial plane waves appear in the case of a spheroid.

REFERENCES

[1] Cpence, R. and Ganger, S. The scattering of sound from a prolate spheroid, *Journal of the Acoustical Society of America*, **23** (6), 701–706, (1951). DOI:10.1121/1.1906827

[2] Burke, J. E. Long-wavelength scattering by hard spheroids, *Journal of the Acoustical Society of America*, **39** (5), 826–831, (1966). DOI:10.1121/1.1909959

[3] Kleshchev, A. A. and Sheiba, L. S. Scattering of a sound wave by ideal prolate spheroids, *Soviet Physic Acoustic*, **16** (2), 219–222, (1970).

[4] Fedoryuk, M. V. Scattering of sound wave from thin acoustically rigid revolve body, *Soviet Physic Acoustic*, **27** (4), 605–609, (1981).

[5] Boiko, A. I. Scattering of plane sound wave from thin revolve body, *Soviet Physic Acoustic*, **29** (3), 189–191, (1983).

[6] Werby, M. F. and Green, L. H. Correspondence between acoustical scattering from spherical and end-on incidence spherical shells, *Journal of the Acoustical Society of America*, **81** (2), 783–787, (1987). DOI:10.1121/1.394796

[7] Veksler, N. D., Dubus, B., and Lavie, A. Acoustic wave scattering by an ellipsoidal shell, *Acoustical Physics*, **45** (1), 46–51, (1999).

[8] Guyer, R. A. and Johnson, P. A. Nonlinear mesoscopic elasticity evidence for a new class of materials, *Physics Today*, **52** (4), 30–36, (1999). DOI:10.1063/1.882648

[9] Lebedev, A. V., Ostrovskii, L. A., and Sutin, A. M. Nonlinear acoustic spectroscopy of local defects in geomaterials, *Acoustical Physics*, **51** (1), S88–S101, (2005).

[10] Abbasov, I. B. Study of the scattering of nonlinearly interacting plane acoustic waves by an elongated spheroid, *Journal of Sound and Vibration*, **309** (1–2), 52–62, (2008). DOI:10.1016/j.jsv.2007.03.060

[11] Skudrzyk, E. *The Foundations of Acoustics*, Vol. 2, Springer, New York, (1971).

[12] Tikhonov, A. N. and Samarskyi, A. A. *The Equations of Mathematical Physics*, Nauka, Moscow, (1966).

[13] Novikov, B. K., Rudenko, O. V., and Timoshenko, V. I. *Nonlinear Underwater Acoustic*, Acoustical Society of America, New York, (1987).

[14] Lyamshev, L. M. and Sakov, P. V. Nonlinear scattering of sound from an pulsted sphere, *Soviet Physics Acoustics*, **38** (1), 50–54, (1992).

[15] Korn, H. and Korn, T. *Mathematical Handbook for Scientists and Engineers*, McGraw-Hill, (1961).

[16] Abbasov, I. B. *Scattering nonlinear interacting acoustic waves: sphere, the cylinder and a spheroid*, Fizmatlit, Moscow, (2007).

[17] Abramovitz, M. and Stegun, I. *Handbook of Special Functions with Formulas, Graphs, and Mathematical Tables*, Dover, New York, (1971).

[18] Prudnikov, A. P., Brychkov, Yu. A., and Marichhev, O. I. *Integrals and series*, Nauka, Moscow, (1983).

[19] Chertock, G. Sound radiation from circular pistons of elliptical profile, *Journal of the Acoustical Society of America*, **33** (7), 871–8876, (1961). DOI:10.1121/1.1908831

[20] Kleshchev, A. A. and Rostovtsev, D. M. Scattering of sound from elastically and liquidly ellipsoidal revolve shell, *Soviet Physic Acoustic*, **32** (5), 432–433, (1986).

[21] Abbasov, I. B. and Zagrai, N. P. Sphere scattering of nonlinear interacting acoustic waves, *Fluid Dynamics*, **30** (2), 158–165, (1995).

[22] Abbasov, I. B. and Zagrai, N. P. The investigation of the second field of the summarized frequency originated from scattering of nonlinearly interacting sound waves at a rigid sphere, *Journal of Sound and Vibration*, **216** (1), 194–197, (1998). DOI:10.1006/jsvi.1998.1638